International Forum on Aeroelasticity and Structural Dynamics
IFASD 2017
25-28 June 2017 Como, Italy

DELAYED DES IN SU2: TEST CASE 3 FROM THE SECOND AIAA AEROELASTIC PREDICTION WORKSHOP

Eduardo S. Molina[1], Cleber Spode[1], Roberto Gil A. da Silva[1], Marcello Righi[2], Thomas D. Economon[3], Juan J. Alonso[3]

[1]ITA - Instituto Tecnológico de Aeronáutica, São José dos Campos, Brasil

[2]Zurich University of Applied Sciences, Winterthur, Switzerland

[3]Stanford University, Stanford, CA 94305, U.S.A.

Keywords: BSCW, DDES, Shock Buffet

Abstract: An extension of Delayed Detached-Eddy Simulation (DDES) capabilities developed in SU2 to unsteady transonic buffet flow is present. An assessment of Spalart-Allmaras turbulence model variants with the 2D OAT15 airfoil reveals that the mixing layer compressibility correction plus the quadratic constitutive relation (SA-Comp-QCR) was the combination able to capture shock buffet accurately. Refined Roe scheme was also implemented, including adaptive dissipation function with Ducros shock sensor and Travin's blending. The SU2 DDES implementation is tested in the Benchmark Supercritical Wing, analyzing the case 3 of the Second AIAA Aeroelastic Prediction Workshop. The results obtained are encouraging, showing good agreement for mean pressure coefficient and coherent fluid flow structures behind the shock.

1 INTRODUCTION

The Second AIAA Aeroelastic Prediction Workshop [1] (AePW-2) was launched with the aim of assessing the quality of numerical predictions of state of art CFD solvers. Three test cases were selected among the experiments carried out by NASA in the TDT wind tunnel with the Benchmark Supercritical Wing (BSCW). The test cases involve three different transonic flow conditions, with Mach numbers ranging from 0.70 to 0.85, and Reynolds around 5×10^6 and angle of attack $3°$, $0°$ and $5°$, respectively. The interaction between the shock waves and the boundary layer is an important feature of the flow in all test cases. In test cases 1 and 2 the boundary layer is attached, but it separates behind the shocks on the upper and lower sides in test case 3.

Different configurations and setups are considered: (i) the oscillating turntable (OTT) providing pitch oscillations around the 30% chord axis, (ii) the pitch and plunge apparatus (PAPA) providing a virtually rigid motion with two degrees of freedom and (iii) the rigid mount.

This study is an extension of the Delayed Detached Eddy Simulation (DDES [2]) implementation in the open-source solver SU2 [3] carried out by the authors and submitted to the AIAA AVIATION 2017 conference. Unsteady and aeroelastic results obtained by the authors with different solvers, including SU2, were previously presented [4]. A summary of all results for the aeroelastic prediction workshop has also been published [5].

Traditionally, aeroelasticians rely on URANS simulations even in flow conditions where the applicability of such a flow model may be questionable [6]. Hybrid RANS/LES modelling is still an evolving technique which has shown encouraging results for flows characterized by large-energy-carrying turbulent length scales [7]. Applications to compressible flows are not yet very popular; however a few good examples can be found in the literature [8, 9]. The application of a hybrid RANS/LES method such as DDES for transonic separated flows is not straightforward: temporal and spatial resolutions must be carefully set in order to capture all relevant scales. In addition,the work of the turbulence model and its "interaction" with the computational grid falls under closer scrutiny: is the RANS model sufficiently "shielded" in the attached flow regions? Is resolved turbulence physically consistent? Is the "gray area" (region of the flow domain where the modelling transitions from RANS to LES) confined to a reasonably small region? An examination of all these challenges and potential benefits is the subject of this work.

This paper continues in Section 2 with a description of the numerical method implemented, in Sections 3 and 4 where two validation cases are presented, and in Section 5, where conclusions are proposed.

2 WORK DESCRIPTION

2.1 Unsteady Flow Solver

The SU2 software suite [3] is an open-source collection of software tools written in C++ and Python designed for multi-physics simulation and design. It is built specifically for the analysis of partial differential equations (PDEs) and PDE-constrained optimization problems on unstructured meshes with state-of-the-art methods. It is particularly well suited for aerodynamic shape design. The finite volume method (FVM) [10] is applied on arbitrary unstructured meshes using a standard edge-based data structure on a dual grid with control volumes constructed using a median-dual, vertex-based scheme. Regarding time integration, SU2 is capable to solve implicitly [11] steady and unsteady problems, using a dual-time stepping strategy [12] and leading to second-order accuracy in space and time.

2.2 Turbulence Modeling

Various options for turbulence modeling are included in the SU2 framework. In this work we focus on the following:

Spalart-Allmaras (SA) Model. In addition to the traditional Spalart-Allmaras (SA) [13] turbulence model, several variants tailored to flows with shock/boundary layer interaction have been implemented including the Edwards & Chandra modification (SA-Edwards) [14], the Mixing Layer Compressibility Correction (SA-Comp) [15] and the Quadratic Constutive Relation (SA-QCR) [16].

Delayed DES. The Delayed Detached Eddy Simulation (DDES) [2] model was implemented in SU2 by Molina et al [17]. It is based on the SA model and its variants. To overcome the slow transition from RANS to LES in shear-layer flows by reducing the so-called "gray area", different recently-proposed modifications of the sub-grid length scale (SGS) were converted to handle unstructured grids: these include both Vorticity Adapted SGS [18] and the Shear-Layer Adapted SGS [19, 20].

2.3 Numerical Methods

In this study, the widely used upwind Roe scheme [21] is used. This scheme has the ability of capture shock waves, but suffers from high dissipation levels that can eliminate most of the small-scale flow structures. In order to resolve turbulent motions and maintain the shock-capturing capability of the Roe scheme, an adaptive dissipation function is introduced. Following the ideas of Xiao et al. [22]:

$$\tilde{F}^c_{ij} = \left(\frac{\vec{F}^c_i + \vec{F}^c_j}{2}\right) \cdot \vec{n}_{ij} - \sigma \left\{\frac{1}{2} P|\Lambda|P^{-1}(U_i - U_j)\right\} - (\vec{u}_{\Omega_{ij}} \cdot \vec{n}_{ij}) \left(\frac{U_i + U_j}{2}\right) \qquad (1)$$

where $\sigma = \sigma_{Ducros} + \sigma_{NTS} - \sigma_{Ducros}\sigma_{NTS}$. σ_{Ducros} and σ_{NTS} are the Ducros' [23] shock sensor and the Travin's [24] numerical blending, respectively.

3 2D OAT15A TRANSONIC BUFFET VALIDATION TEST CASE

3.1 Test Description

The transonic buffet over the OAT15a was investigated experimentally by Jacquin et al. [25] at free-stream Mach numbers in the range of $0.70 - 0.75$ and a chord-based Reynolds number of $3 \cdot 10^6$. The OAT15a is a supercritical wing section with a thickness-to-chord ratio of 12.3%. The wind-tunnel model has a chord of $C = 0.23$ m, trailing edge thickness is $0.005C$ and the boundary-layer was tripped at $0.07x/C$ from the leading edge for a fully turbulent behavior, the detailed experimental set-up can be found in Jacquin et al [25]. The results showed that a periodic self-sustained shock-wave motion was obtained for angles of attack higher than 3.5 degrees at a fix Mach number of $M = 0.73$ and the buffet frequency was found to be $69 - 70$Hz. In order to analyse the capability in predict the buffet onset through unsteady RANS simulations, the flow is considered in two dimensions at an angle of attack of $\%3.5$ and free-stream Mach number of $M = 0.73$.

3.2 Numerical Setup

The considered grid has a H topology with 170 000 cells approximately and a domain size of 40 chords. The shock resolution (maximum element) over the airfoil is $0.005c$. The y^+ coordinate is smaller than 0.75. Figure 1 shows the grid near the airfoil.

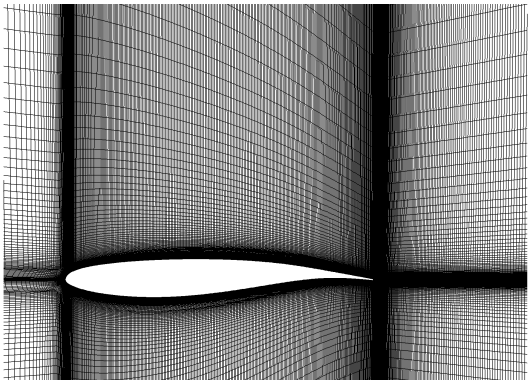

Figure 1: Close view of the computational grid.

The convective fluxes were discretized using the standard Roe, $\sigma = 1.0$ in Eq.1, whereas the convective fluxes of the turbulence model equation were treated with a first-order Roe scheme.

A study of the influence of the chosen time-step has been carried out with the present grid, it was noted that periodic shock-wave motion was captured with time steps smaller than $5 \cdot 10^{-4} C/U_\infty$. Deck [8] and Szubert et al [26] also found a similar time-step in their convergence study. The number of inner iterations in the dual time-step strategy and the number of the linear solver (Krylov subspace) iterations were set to 5.

3.3 Results

Based on previous simulations, not shown here, in order to analyse the buffet onset prediction capability of the already available turbulence models in SU2 and the others specially implemented for the present study. It was shown that the Spalart-Allmaras (SA) [13] in its standard version and the two equation $k-\omega$ SST model [27] were not able to produce any shock motion at the present incidence. The Spalart-Allmaras model with mixing layer compressibility correction (SA-Comp) [15] underpredicted the amplitudes of the shock motion. The SA-Comp model with the Quadratic Constitutive Relation (SA-Comp-QCR) [16] was able to produce the self-sustained shock motion with a frequency close to the experimental. The results can be observed in Fig. 2 for the evolution of the lift coefficient.

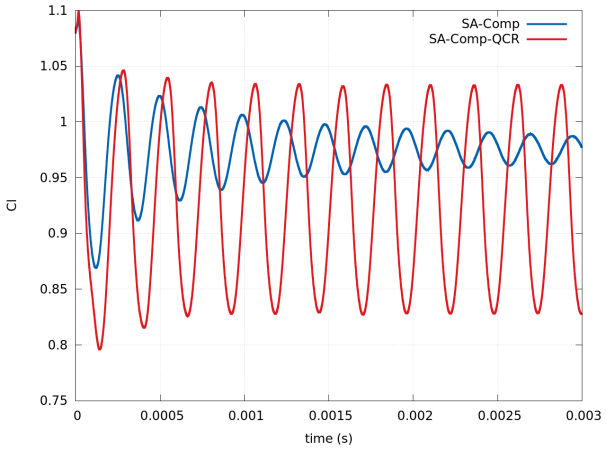

Figure 2: Comparison of the time evolution of the lift coefficient between the Spalart-Allmaras model using compressibility corrections (SA-Comp) without and with Quadratic Constitutive Relation (SA-Comp-QCR).

A turbulence model comparison is provided in Fig. 3. The mean value of the pressure coefficient (Fig. 3 left) and the RMS pressure distribution over the airfoil (Fig. 3 right) obtained using the SA-Comp-QCR model are in good agreement with the experimental data in terms of shock motion and unsteady pressure amplitude. On the other hand, the results obtained with SA-Comp underpredicted the RMS pressure amplitude and the shock motion.

In addition, the SA-Comp-QCR model captured the formation of secondary oscillations within the buffet cycles, mainly due to intermittent von Kármán vortex shedding, similar results were obtained by Szubert et al. [26] using the $k-\epsilon$-OES model. Figure 4 presents the density gradient magnitude for the SA-Comp and SA-Comp-QCR turbulence models. As one can see, the shear-layer and trailing edge instabilities are only captured with the SA-Comp-QCR model (Fig. 4 right). The difference of the QCR relies on the fact that the classical linear Boussinesq approximation failed to predict secondary corner and/or junction flows [28]. To circunvent this limitation, Spalart proposed the QCR by adding a second nonlinear term to the linear Reynolds stress tensor to account for the anisotropic, Reynolds-stress behavior in corner flows [16, 29]. To the authors' knowledge this is the first study ever to combine the QCR relation with unsteady transonic flow simulations.

4 3D BSCW TEST CASE

4.1 Test Description

The Benchmark Supercritical Wing (BSCW) consists of a rectangular supercritical wing tested at NASA Transonic Dynamics Tunnel, as shown in Figure 5. The experimental set-up involved two different configurations. In the first configuration, the wing was mounted on the oscillating turntable (OTT), which provided forced pitch oscillation data. In the second configuration, the wing was mounted on a flexible pitch and plunge apparatus (PAPA), where the mount system provides low-frequency flexible modes that emulate a pitch and plunge modes. In each test, the model was mounted to the same splitter plate that placed it well outside the wind-tunnel boundary layer, as seen in Figure 5. The instrumentation of the model consists of only a single row of unsteady pressure transducers located at 60% of the span location.

A summary of the AePW-2 test cases are presented in table 1. While Test Cases 1 and 2 concern the response of the BSCW wing in transonic attached flow. Test Case 3, $M = 0.85$ and 5° angle-of-attack, is a complex and challenging test case including a strong shock-wave/boundary layer interaction with flow separation. In this study, Test Case 3a is analysed by means of a hybrid RANS/LES approach, based on the SA-DDES model.

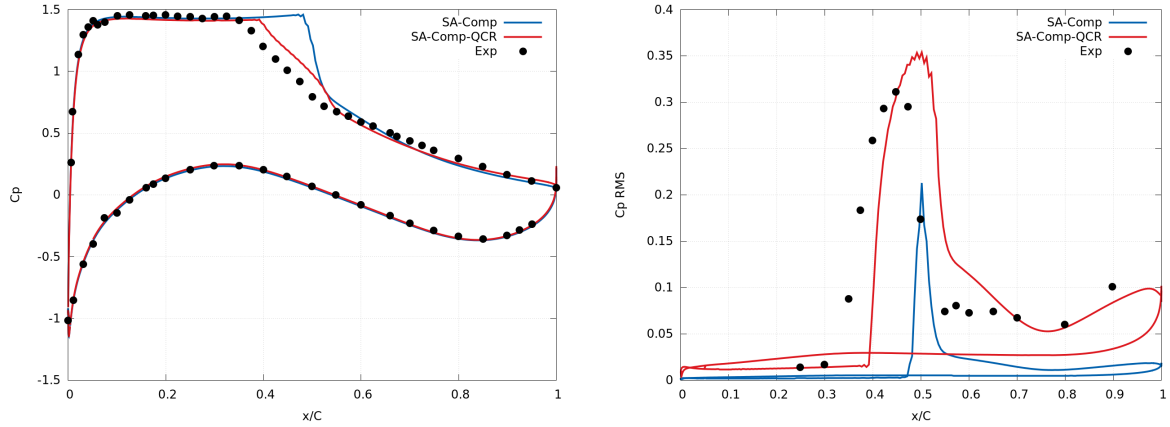

Figure 3: Turbulence model comparison of the mean pressure coefficient (left) and the RMS of the pressure coefficient (right). Experiment by Jacquin et al. [25].

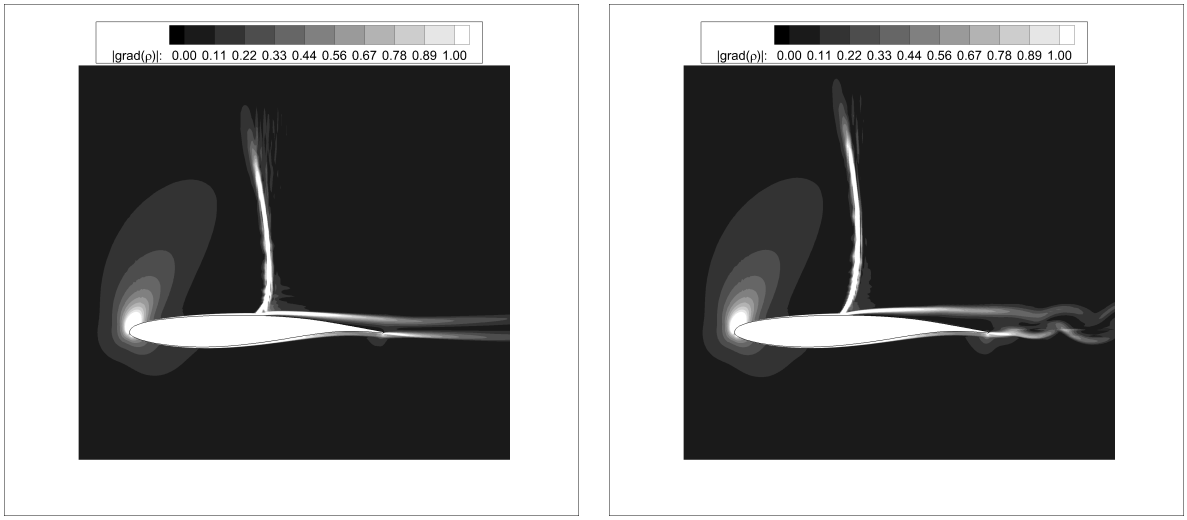

Figure 4: Instantaneous fields of density gradient magnitude: SA-Comp (left), SA-Comp-QCR (right)

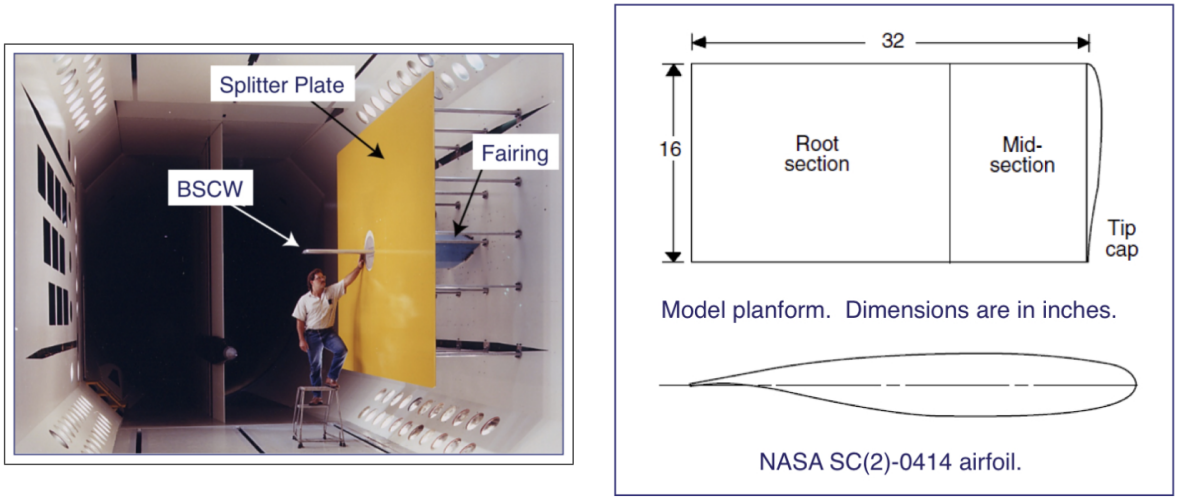

Figure 5: Benchmark Supercritical Wing (BSCW) geometry definition.

Table 1: AePW-2 Test Cases

	Case 1	Case 2	Case 3A	Case 3B	Case 3C
Mach	0.70	0.74	0.85	0.85	0.85
AoA	3.0°	0.0°	5.0°	5.0°	5.0°
Reynolds Number	$3.418e6$	$4.450e6$	$4.491e6$	$4.491e6$	$4.491e6$
Dynamic Data Type	Forced Oscillation $f = 10Hz, \lvert\Theta\rvert = 1°$	Flutter	Unforced Unsteady	Forced Oscillation $f = 10Hz, \lvert\Theta\rvert = 1°$	Flutter
Notes:	-Attached flow -OTT exp. data -R-134a	-Flow state(?) -PAPA exp. data -R-12	-Separated flow -OTT exp. data -R-134a	-Separated flow -OTT exp. data -R-134a	-Separated flow No exp. dat -R-134a

4.2 Numerical Setup

For scale-resolving simulations, a refined mesh is needed in order to resolve the turbulent structures present in the separate zone. Typically in external aeronautical applications, the separated flow represents only a small portion of the entire flow field. Thus, in order to limit the cell count, a hybrid grid containing tetrahedra, prism and hexahedra on the volume mesh was created refining the region of interest. The surface grid consists of triangles on the wing tip and quadrilaterals on the upper/lower wing. Whereas the volume mesh contains prisms and hexahedra inside the boundary layer, a block of structured cells was placed in the wake region. The connection of the boundary layer with the wake block and the rest of the domain is done by using pyramids and tetrahedra cells. The y^+ coordinate is smaller than 0.75 everywhere.

Based on the previous 2D OAT15a test case results, both the surface grid of the upper/lower wing and the volume grid of the structured block inside the wake have a maximum resolution of $0.005c$ in all spatial dimensions. The total amount of computational cells is about 39 million cells.

The convective fluxes were discretized using the Roe scheme with an adaptive dissipation function, Eq.1, whereas the convective fluxes of the turbulence model equation were treated with a first-order Roe scheme.

The DDES model based on the SA turbulence model was used in the present study. The underlying SA variant model is the previously used SA-Comp-QCR. The chosen DDES length scale is the vorticity-based ($\Delta = \Delta_\omega$) which was proven to perform a faster transition from RANS to LES compared to the standard DDES length scale ($\Delta = \Delta_\omega$) [17]. The chosen time step was

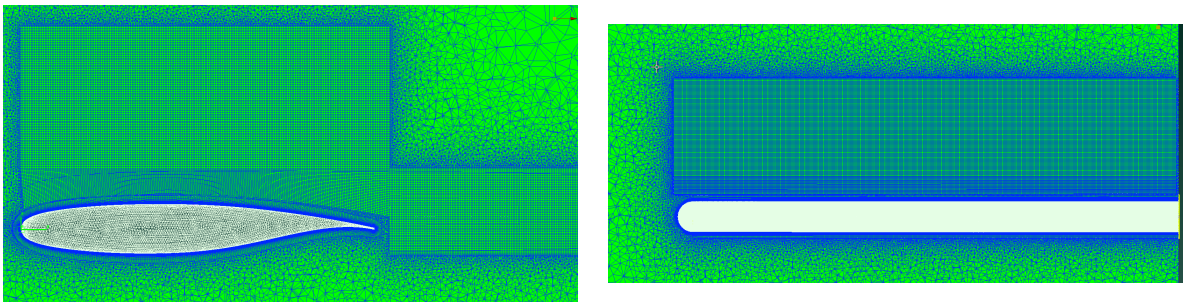

Figure 6: Close view of the computational grid.

$1 \cdot 10^{-2} C/U_\infty$. The number of inner iterations in the dual time-step strategy and the number of the linear solver (Krylov subspace) iterations were set to 7.

The simulation was run on Euler-CeMEAI-USP on 600 cores. The total simulation time is 60000 time steps, corresponding 600 times the convective time scale, and it lasts 18 days.

4.3 Results

The instantaneous adaptive numerical dissipation function is presented in Fig.7(left). The adaptive function is designed to be one away from the wall including the shock-wave region whereas it is designed to effectively reduce the dissipation ($\sigma \approx 0$) in the shear layer/wake region. Figure 7(right) shows the instantaneous density gradient flow field where a pronounced lambda shock is observed and the interaction between together with the interaction between large-scale turbulent structures and the trailing edge.

The richness of topological coherent fluid structures of the present shock buffet flow is noticed on the Q-criterion plot of Figure 8, proving the ability of hybrid RANS/LES method to capture such complex phenomena.

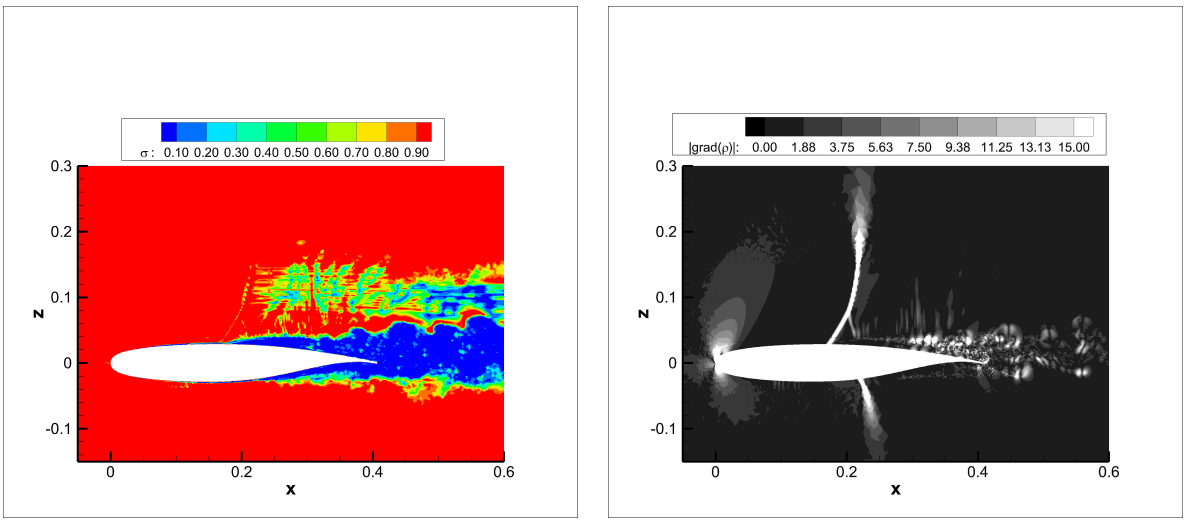

Figure 7: Instantaneous fields: Adaptive dissipation function (left) and density gradient magnitude (right).

Figure 9 presents the average spatial distribution of the pressure coefficient, evaluated at the surface of the wing. Upper (Fig9(left)) and lower (Fig9(right)) surfaces present a pronounced shock wave/boundary layer interaction at the present incidence.

During the unsteady simulation, the RMS of the fluctuating pressure is calculated to access

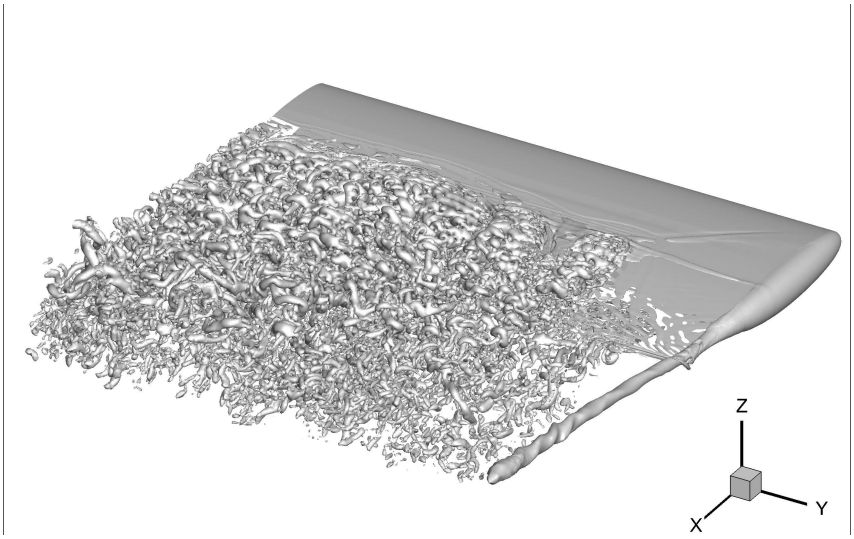

Figure 8: Perspective of DDES showing iso-surface of Q-criterion $100 * c^2/U_\infty^2$.

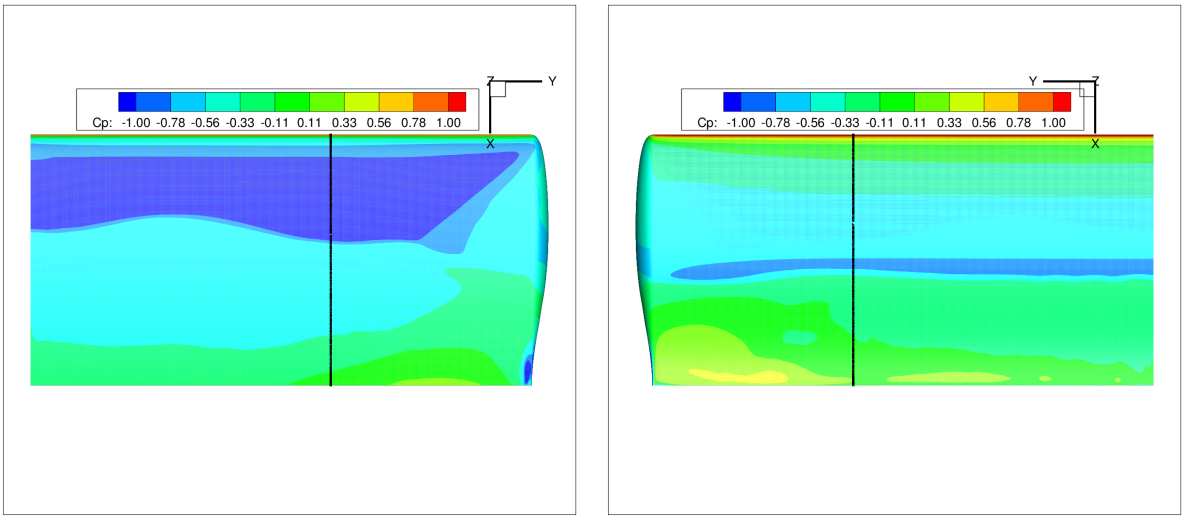

Figure 9: Upper (left) and lower (right) surface mean pressure coefficient distribution.

the spatial distribution of the unsteadiness of the flow. Figure 10 presents the RMS pressure evaluated at the upper (Fig.10 (left)) and lower upper (Fig.10 (right)) surfaces. In both surfaces, the shock foot is characterized by high values of pressure fluctuation. A similar shock-foot trace was observed in the DDES transonic buffet simulation of a wing-body configuration performed by Sartor & Timme [30] and in unsteady RANS simulations of a infinite sweep wing for various sweep angles [31]. On the upper surface, two zones of high pressure fluctuations are visible besides the shock trace whereas on the lower surface, a single separated zone near the trailing edge is visible.

Figure 11 (left) presents the comparison of the mean pressure coefficient with the available experimental data. Comparing DDES and RANS results, DDES results are in better agreement with the experimental data. Although, the shock moves upstream, the prediction of the separated zone downstream of the shock is improved using DDES. This is consistent with the observation of the mean lift coefficients, summarized in Table 2, where DDES results is lower than steady RANS.

The RMS pressure coefficient comparison between DDES simulation and experimental data is

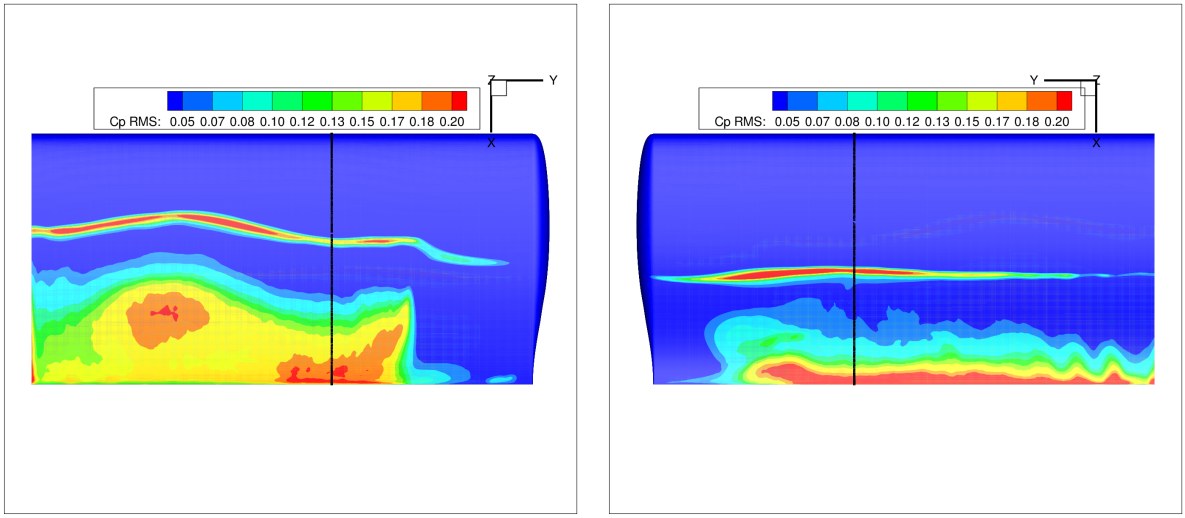

Figure 10: Upper (left) and lower (right) surface RMS pressure coefficient distribution.

showed in Fig.11(right), the amplitude of shock unsteadiness is fairly captured whereas the pressure fluctuations downstream of the shock are over-predicted. A possible cause for this over-prediction is the very low eddy viscosity given by the vorticity-based length scale. Deck [18] argued that the use of the vorticity-based length scale can worsen the modeled stress depletion, a possible way to circumvent this tendency is to take advantage of the f_d DDES function that can be used as blend from $\Delta = \Delta_{max}$ (inside the boundary layer) to $\Delta = \Delta_{\omega}$ (suited to ensure a rapid transition from RANS to LES) [17, 18].

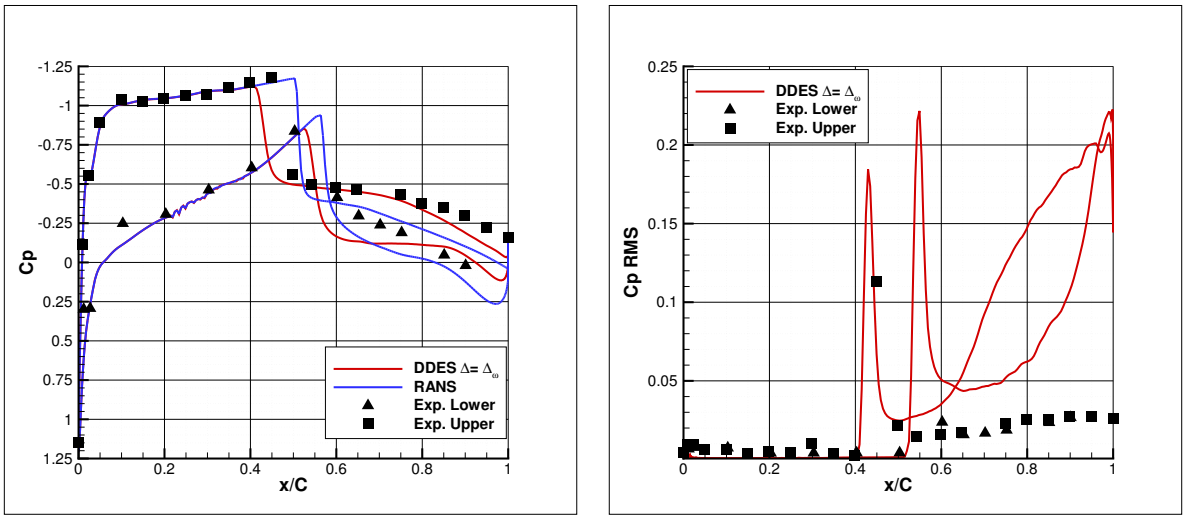

Figure 11: Comparison between calculated and measured mean (left) and RMS (right) pressure coefficient at 60% of span.

Table 2: Mean and RMS values of lift and drag coefficients.

	Mean lift	RMS lift	Mean drag	RMS drag
RANS	0.3689	-	0.0707	-
DDES	0.3397	9.074E-03	0.0740	8.424E-04

The frequency content of the DDES simulation, presented in Fig.12, is discussed by analyzing the power spectral density (PSD) of the lift coefficient. As already mentioned by Deck [8] and Sartor & Timme [30], unsteady hybrid RANS/LES simulations have a short time dura-

tion, consequently the signal is oversampled, leading to a noise PSD when using the traditional fast Fourier transform due to the small number of averages. Instead of using the well-know Welch periodogram, the autoregressive PSD using the Burg method is used. From the results of both PSD methods, the peak is broadband indicating nonperiodic shock motions without any significant peak in the high-frequency range.

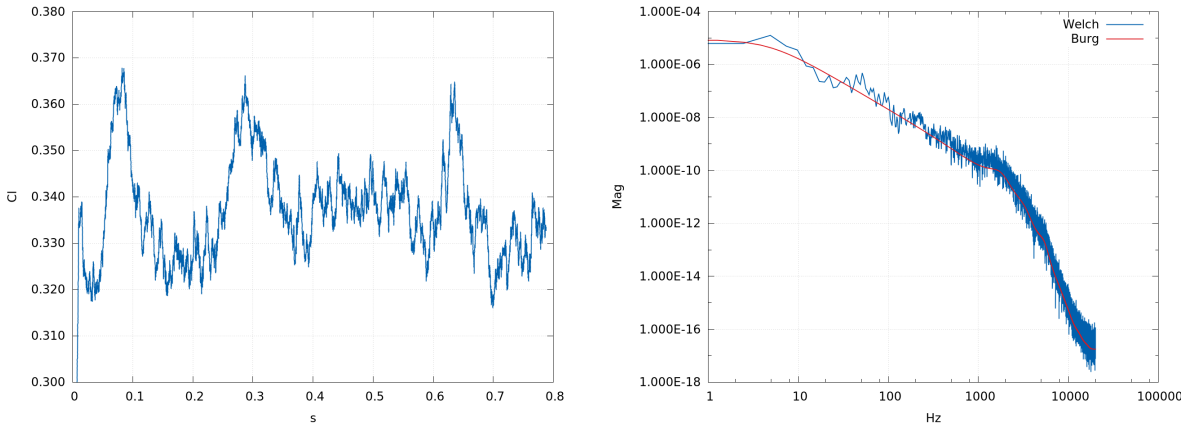

Figure 12: Time history of lift coefficient (left) and power spectral density of lift coefficient (right).

5 CONCLUSION

The aim of the present study was to extend the Delayed Detached-Eddy Simulation (DDES) capabilities of SU2 to unsteady transonic flows. The 2D OAT15a airfoil test case was used as a standard unsteady Reynolds-average Navier-Stokes (URANS) validation of the underlying turbulence model implementation, different Spalart-Allmaras turbulence model variants were implemented for the present study, however, the only variant that was able to capture shock buffet accurately was the Spalart-Allmaras with mixing layer compressibility correction and quadratic constitutive relation (SA-Comp-QCR). The Benchmark Supercritical Wing (BSCW), Test Case 3a from the 2nd Aeroelastic Prediction Workshop, was selected for the DDES simulations.

Concerning the DDES results, the unsteady separated zone extends from the symmetry plane until almost the wing tip and the shock unsteadiness is characterized by nonperiodic shock motions. The comparison with the available experimental data showed a good agreement of the mean pressure coefficient and an overpredicted pressure fluctuation downstream of the shock.

Although, the results obtained so far are (at least) encouraging, demonstrating that the hybrid models have been implemented correctly, the role played by numerical dissipation in SU2 still must be quantified. Furthermore, gray area mitigation measures appear to play an important role in hybrid modeling.

6 ACKNOWLEDGEMENTS

The authors from ITA are grateful to CeMEAI/USP (http://www.cemeai.icmc.usp.br/) for providing the computational resources.

7 REFERENCES

[1] Heeg, J., Chwalowski, P., Schuster, D. M., et al. (2015). Plans and example results for the 2nd aiaa aeroelastic prediction workshop. In *56th AIAA/ASCE/AHS/ASC Structures, Structural Dynamics, and Materials Conference*. p. 0437.

[2] Spalart, P., Deck, S., Shur, M., et al. (2006). A new version of detached-eddy simulation, resistant to ambiguous grid densities. *Theoretical and Computational Fluid Dynamics*, 20(3), 181–195. ISSN 0935-4964. doi:10.1007/s00162-006-0015-0.

[3] Economon, T. D., Palacios, F., Copeland, S. R., et al. (2015). Su2: An open-source suite for multiphysics simulation and design. *AIAA Journal*, 54(3), 828–846. doi: 10.2514/1.J053813.

[4] Righi, M. (2016). RANS-LES Hybrid Turbulence Modelling for Aeroelastic Problems: Test Case 3 in the Second AIAA Aeroelastic Prediction Workshop. *AIAA-2016-2861*.

[5] Heeg, J., Wieseman, C. D., and Chwalowski, P. (2016). Data comparisons and summary of the second aeroelastic prediction workshop. *AIAA-2016-...*

[6] Bendiksen, O. O. (2011). Review of unsteady transonic aerodynamics: Theory and applications. *Progress in Aerospace Sciences*, 47(2), 135–167.

[7] Girimaji, S., Haase, W., Peng, S. H., et al. Progress in hybrid RANS-LES modelling.

[8] Deck, S. (2005). Numerical simulation of transonic buffet over a supercritical airfoil. *AIAA journal*, 43(7), 1556–1566.

[9] Barbut, G., Braza, M., Hoarau, Y., et al. (2010). Prediction of transonic buffet around a wing with flap. In *Progress in Hybrid RANS-LES Modelling*. Springer, pp. 191–204.

[10] LeVeque, R. (2002). *Finite Volume Methods for Hyperbolic Problems*. Cambridge Univesity Press.

[11] Saad, Y. and Schultz, M. H. (1986). GMRES: A generalized minimal residual algorithm for solving nonsymmetric linear systems. *SIAM J. Sci. Stat. Comput.*, 7, 856–869.

[12] Jameson, A. and Schenectady, S. (2009). An assessment of dual-time stepping, time spectral and artificial compressibility based numerical algorithms for unsteady flow with applications to flapping wings. *AIAA Paper 2009-4273*.

[13] Spalart, P. and Allmaras, S. (1992). A one-equation turbulence model for aerodynamic flows. In *AIAA Paper 1992-0439*.

[14] Edwards, J. R. and Chandra, S. (1996). Comparison of eddy viscosity-transport turbulence models for three-dimensional, shock-separated flowfields. *AIAA Journal*, 34(4), 756–763. ISSN 0001-1452, 1533-385X. doi:10.2514/3.13137.

[15] Spalart, P. (2000). Trends in turbulence treatments. In *AIAA Fluids Conference and Exhibit*. p. 2306.

[16] Spalart, P. R. (2000). Strategies for turbulence modelling and simulations. *International Journal of Heat and Fluid Flow*, 21(3), 252–263.

[17] Molina, E., Spode, C., da Silva, R., et al. (2017). Hybrid RANS/LES in SU2. In *23th AIAA Computational Fluid Dynamics Conference*.

[18] Deck, S. (2012). Recent improvements in the Zonal Detached Eddy Simulation (ZDES) formulation. *Theoretical and Computational Fluid Dynamics*, 26(6), 523–550. ISSN 0935-4964, 1432-2250. doi:10.1007/s00162-011-0240-z.

[19] Shur, M. L., Spalart, P. R., Strelets, M. K., et al. (2015). An enhanced version of des with rapid transition from rans to les in separated flows. *Flow, Turbulence and Combustion*, 95(4), 709–737. ISSN 1573-1987. doi:10.1007/s10494-015-9618-0.

[20] Guseva, E. K., Garbaruk, A. V., and Strelets, M. K. (2016). Assessment of delayed des and improved delayed des combined with a shear-layer-adapted subgrid length-scale in separated flows. *Flow, Turbulence and Combustion*, 1–22. ISSN 1573-1987. doi: 10.1007/s10494-016-9769-7.

[21] Roe, P. L. (1981). Approximate Riemann solvers, parameter vectors, and difference schemes. *Journal of computational physics*, 43(2), 357–372.

[22] Xiao, L., Xiao, Z., Duan, Z., et al. (2015). Improved-delayed-detached-eddy simulation of cavity-induced transition in hypersonic boundary layer. *International Journal of Heat and Fluid Flow*, 51, 138 – 150. ISSN 0142-727X. doi: http://dx.doi.org/10.1016/j.ijheatfluidflow.2014.10.007. Theme special issue celebrating the 75th birthdays of Brian Launder and Kemo Hanjalic.

[23] Ducros, F., Ferrand, V., Nicoud, F., et al. (1999). Large-eddy simulation of the shock/turbulence interaction. *Journal of Computational Physics*, 152(2), 517–549.

[24] Travin, A., Shur, M., Strelets, M. M., et al. (2002). Physical and numerical upgrades in the detached-eddy simulation of complex turbulent flows. In *Advances in LES of complex flows*. Springer, pp. 239–254.

[25] Jacquin, L., Molton, P., Deck, S., et al. (2009). Experimental study of shock oscillation over a transonic supercritical profile. *AIAA journal*, 47(9), 1985–1994.

[26] Szubert, D., Grossi, F., Garcia, A. J., et al. (2015). Shock-vortex shear-layer interaction in the transonic flow around a supercritical airfoil at high reynolds number in buffet conditions. *Journal of Fluids and Structures*, 55, 276–302.

[27] Menter, F. R. (1994). Two-equation eddy-viscosity turbulence models for engineering applications. *AIAA journal*, 32(8), 1598–1605.

[28] Dandois, J. (2014). Improvement of corner flow prediction using the quadratic constitutive relation. *AIAA journal*, 52(12), 2795–2806.

[29] Leger, T., Bisek, N., and Poggie, J. (2016). Supersonic corner flow predictions using the quadratic constitutive relation. *AIAA Journal*, 54(7), 2077–2088.

[30] Sartor, F. and Timme, S. (2016). Delayed detached–eddy simulation of shock buffet on half wing–body configuration. *AIAA Journal*, 1–11.

[31] Iovnovich, M. and Raveh, D. E. (2014). Numerical study of shock buffet on three-dimensional wings. *AIAA Journal*, 53(2), 449–463.